A Quantum Chemistry Based Force Field for Poly(dimethylsiloxane)

James S. Smith,* Oleg Borodin, and Grant D. Smith

Department of Material Science and Engineering and Department of Chemical Engineering, University of Utah, 122 South Central Campus Drive Room 304, Salt Lake City, Utah 84112

Received: June 14, 2004; In Final Form: September 9, 2004

A classical force field for poly(dimethylsiloxane) (PDMS) and its oligomers has been derived on the basis of intermolecular binding energies, molecular geometries, molecular electrostatic potentials, and conformational energies obtained from quantum chemistry calculations on model compounds. The force field accurately reproduces the molecular properties of the model compounds obtained from quantum chemistry, including the Si−O−Si bond linearization energy. Molecular dynamics simulations performed on PDMS of various molecular weights between 310 and 1571 using the quantum chemistry based force field yielded good agreement with experiment for their densities, enthalpies of vaporization, and X-ray structure factors. The characteristic ratio of PDMS was also found to be in good agreement with experimental values. Molecular dynamics as represented by the melt self-diffusion coefficient and viscosity at 298 K as a function of molecular weight were also found to be in reasonable agreement with experimental values. Finally, the intermediate incoherent structure factor of PDMS from MD simulations was in excellent agreement with the quasi-elastic neutron scattering results for large *Q* values and in satisfactory agreement for small *Q* values.

I. Introduction

Poly(dimethylsiloxane) (PDMS) is representative of the industrially important silicone polymers. PDMS itself has an extremely low glass transition temperature and viscosity that have been attributed to chain flexibility, weak intermolecular interactions, and relatively free motion of its side groups.[1] PDMS has applications as an oil, resin, and elastomer, and when combined with micro- and nanoscopic silica particles, forms strong elastomers.[2] Gaining a molecular-level understanding of PDMS is important in explaining the unique physical properties of PDMS and the interfacial interactions with nanoscopic particles[3] that produce such dramatic increases in strength.

Fundamental to the properties of silicones is the presence of the alternating silicon and oxygen atoms in the chain backbone; the long Si−O bond length (1.64 Å compared to 1.53 Å for the typical C−C bond) and lack of side groups on the oxygen create a relatively open intramolecular structure that strongly influences the backbone geometry, bending flexibility, and conformational energetics of silicones as well as the density and cohesive energy compared to those in carbon-based polymers. The conformational flexibility of PDMS is well-known and is believed to be largely responsible for the low glass transition temperature of the polymer. The highly labile Si−O−Si bend in the PDMS backbone may also play an important role in the unique characteristics of PDMS. We have undertaken development of a quantum chemistry based potential designed to reproduce as accurately as possible these unique characteristics. Particular attention has been paid to dispersion/repulsion interactions involving silicon, polar interactions resulting from the electron-donating character of silicon, conformational energetics, and the geometry and linearization energy for the Si−O−Si bend. Below, we describe our quantum chemistry calculations on representative compounds, force field parametrization, and validation of the force field through comparison of thermodynamic, structural, and dynamic properties of PDMS obtained from molecular dynamics (MD) simulations with experiments.

II. Quantum Chemistry Studies of PDMS Model Compounds

A. Previous Quantum Chemistry Studies. Quantum chemistry studies of PDMS model compounds have concentrated on the equilibrium Si−O−Si angle in disiloxane (DS), shown in Figure 1a, and its linearization energy. The linearization energy is defined as the difference between the energy of the optimized (bent) DS geometry and the energy when the Si−O−Si bend angle is linear. Experimental findings vary, giving equilibrium angles from 144° to 180°,[4] but dipole measurements of disiloxane samples indicate that the molecule is bent. Experimental estimates for the linearization energy range from 0.3 to 1.4 kcal/mol.[5] Quantum chemistry studies have yielded equilibrium angles ranging from 138 to 180° with values for the linearization energy ranging from 0.0 to 1.36 kcal/mol,[6] depending upon the level of theory and basis set used. Early quantum chemistry investigations of DS confirmed that d orbitals in the basis sets of the silicon and oxygen atoms were necessary to obtain bent geometries.[7] It was also found that careful orbital adjustment on silicon was needed to correctly reproduce the molecular dipole and bend linearization barrier for small basis sets. Later work showed that such careful adjustments were not needed for the expanded double-ζ and triple-ζ basis sets (DZ+2d and TZ+2d) used with electron correlation.[8] Koput[9] predicted an acceptable bent geometry with double- and triple-ζ type basis sets but only when electron correlation was included, and other investigators also showed that MP2, MP3, and coupled cluster calculations favored bent geometries and increasingly large energy barriers due to increased electron correlation.[6]

B. Bend Linearization Barrier in Disiloxane. Our goal was to establish an adequate level of theory and basis set for quantum chemistry calculations that would accurately reproduce the geometry and linearization energy of DS (Figure 1a) while remaining sufficiently modest to allow us to investigate larger PDMS model compounds needed to establish conformational energies, charge distributions, and molecular weight dependence

10.1021/jp047434r CCC: $27.50
Published on Web 12/02/2004

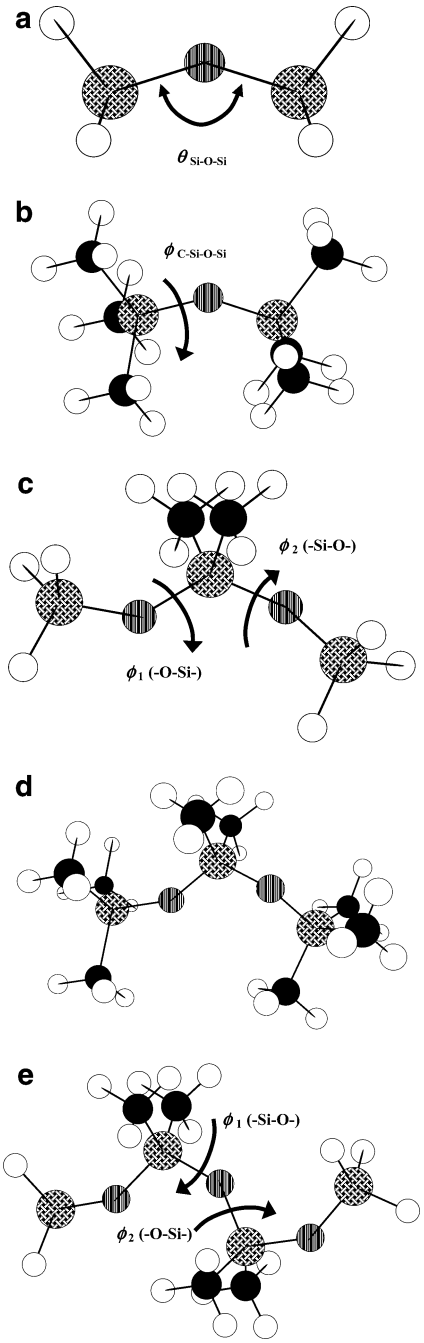

Figure 1. PDMS oligomers, (a) disiloxane (DS), (b) hexamethyldisiloxane (HMDS), (c) 3-dimethyltrisiloxane (DMTS), (d) octamethyltrisiloxane (OMTS), and (e) 3,5-tetramethylsiloxane (TMTS). Solid atoms are carbon, crosshatched are silicon, vertically patterned are oxygen, and plain are hydrogen.

of the linearization energy. This precludes geometry optimization using correlated (e.g., MP2) methods with augmented correlation consistent double-ζ and triple-ζ basis sets, which would simply be too computationally demanding to allow for adequate exploration of the conformational energy surface for PDMS model compounds (see section II.B.).

All quantum chemistry calculations in this study were performed using Gaussian98.[10] In addition to DS, extensive calculations were performed on 3-dimethyltrisiloxane (DMTS, $H_3SiOSi(CH_3)_2OSiH_3$), as well as limited studies of 3,5-tetramethyltetrasiloxane (TMTS, $H_3SiOSi(CH_3)_2OSi(CH_3)_2OSiH_3$), octamethyltrisiloxane (OMTS, $(CH_3)_3SiOSi(CH_3)_2OSi\ (CH_3)_3$), and hexamethyldisiloxane (HMDS, $(CH_3)_3SiOSi(CH_3)_3$), shown in Figure 1.

TABLE 1: Geometry and Bend Linearization Energy for the Si−O−Si Disiloxane Bend

		optimized Si−O−Si	linearization energy (kcal/mol)		
geometry	basis set	angle (degrees)	B3LYP	HF	MP2
HF	6-31G*	165		0.01	0.11
HF	6-31G(2d)	144		0.76	1.16
HF	6-311G(2d)	146		0.71	1.11
HF	6-311G(2df)	168		0.01	0.10
HF	cc-pvDz	151		0.33	1.10
HF	cc-pvTz	167		0.01	0.12
HF	aug-cc-pvDz	140		1.22	2.24
B3LYP	6-31G*	153	0.06	−0.08	0.36
B3LYP	6-31G(2d)	144	0.60	0.71	1.19
B3LYP	6-311G(2d)	142	0.92	0.62	1.25
B3LYP	6-311G(2df)	153	0.11	−0.14	0.36
B3LYP	6-311G(2df,2p)	153	0.11	−0.17	0.11
B3LYP	cc-pvDz	142	0.83	0.10	1.52
B3LYP	cc-pvTz	151	0.22	−0.16	0.39
MP2	6-311G(2df)	147		−0.38	0.41
MP2	cc-pvDz	137		−0.22	1.59
	experimental results[a]				
		151		0.3	

[a] Experimental data from ref 11.

Results of quantum chemistry calculations for the geometry and linearization energy of DS together with a value from Raman experiments[11] are summarized in Table 1. No systematic improvement (agreement with experiment) could be found by increasing the basis set size beyond those shown in Table 1, for example, using correlation consistent polarized valence basis sets or including additional polarization functions, whereas inclusion of electron correlations always increased linearization energy. On the basis of these studies, we concluded that the geometry and linearization energy of DS could be captured at the HF/6-31G(2d) level as accurately as with much larger basis sets and, therefore, used this level of theory in most of our studies of larger PDMS compounds. Selected studies were also performed at the higher MP2/6-311G(2df)//B3LYP/6-311G(2df) level, which also yields good agreement with experiment for the geometry and linearization energy of DS (see Table 1), as described below.

C. Conformational Energetics of 3-Dimethyltrisiloxane. The DMTS molecule has two backbone Si−O−Si−O torsions $\phi_1\phi_2$ as shown in Figure 1c. Quantum chemistry calculations at the HF/6-31G(2d) level yielded an extremely flat DMTS conformational energy surface. The minimum energy Si−O−Si−O $\phi_1\phi_2$ conformation at the HF/6-31G(2d) level was found to be *cis*150 (0.4°, 148.9°), and the maximum energy conformation was found to be a (second-order) saddle point at *tt*[12] with an energy of 1.12 kcal/mol relative to the minimum energy conformation. All stationary points for DMTS are summarized in Table 2. In addition to the stationary points, a large number of conformations with either a single fixed dihedral angle, or with both dihedral angles fixed, were investigated. Energies for these conformers were also calculated at the MP2/6-311G(2df)//B3LYP/6-311G(2df) level (stationary points are given in Table 2). The conformation energy surface is quite similar at the higher level of theory but is somewhat flatter overall. It was found that the Si−O−Si bend spontaneously linearized in DTMS during B3LYP/6-311G(2df) geometry optimizations for conformations approaching *tt*, an effect we believe to be an artifact of the level of theory, which we believe predicts a linearization energy for DS that is too small (see Table 1). For conformations where the Si−O−Si bends linearized (for example, the *tt* conformation), these bends were constrained in the range of 145−147° to allow calculation of the conformational energy.

TABLE 2: Conformational Energy of DMTS at Quantum Chemistry Stationary Points

		conformational energy (kcal/mol)[b] and geometry[c]					
label[a]	state	HF/6-31G(2d)[d]		MP2/6-311G(2df)[e]		force field	
A	min	0.00	0.4, 148.9	0.00	4.9, 165.6	0.01	1, 154
B	saddle	0.02	0, 180	0.02	0, 180	0.00	0, 180
C	saddle[f]	1.12	180, 180	0.51	180, 180	0.83	180, 180
D	saddle[f]	0.90	0, 0	0.26	0, 0	0.17	0, 0
E	saddle	0.08	58.5, 59	−0.21	63.2, 64.1	0.36	58.5, 59[g]
F	saddle	0.45	71.8, 294	0.12	71.8, 294[g]	0.49	71.8, 294[g]

[a] Points labeled in Figure 6. [b] Relative to the minimum energy conformation. [c] ϕ_1, ϕ_2 dihedral angles. [d] Using HF/6-31G(2d) geometries. [e] Using B3LYP/6-311G(2df) geometries. [f] Second-order saddle points (local maxima). [g] Geometry was constrained to the HF/6-31G(2d) saddle-point geometry.

Finally, rotational energetics of both the silyl H−Si−O−Si torsions and methyl H−C−Si−O torsions in DTMS were investigated at the HF/6-31G(2d) level, and both showed threefold rotational symmetry with minimum energies in the staggered conformations.

III. Force Field Parametrization

A. Force Field Form and Development Methodology. In this classical force field the total energy, $U^{TOT}(r)$, of the ensemble of atoms represented by a coordinate vector $\boldsymbol{r}$, is the sum of the nonbonded energy, $U^{NB}(r)$, as well as the energy from the bonds, $U^{BOND}(r_{ij})$, bends, $U^{BEND}(\theta_{ijk})$, and torsions, $U^{TORS}(\phi_{ijkl})$, having bond length r_{ij}, bending angle θ_{ijk}, and dihedral angle ϕ_{ijkl}, respectively.

$$U^{TOT}(r) = U^{NB}(r) + \sum_{ij} U^{BOND}(r_{ij}) + \sum_{ijk} U^{BEND}(\theta_{ijk}) + \sum_{ijkl} U^{TORS}(\phi_{ijkl}) \quad (1)$$

The nonbonded interaction calculations are described in the next section, but it should be noted that the intramolecular 1−4 nonbonded interactions (atoms separated by three bonds) were scaled by 0.5 and that the nonbonded interactions of atom pairs separated by less than three bonds are not evaluated. The nonbonded, bond, bend, and torsional energy for atoms i, j, k, and l having atom types α, β, γ, and δ, respectively, are given by:

$$U^{NB}(r) = \sum_{i<j} A_{\alpha\beta} \exp(-B_{\alpha\beta} r_{ij}) - \frac{C_{\alpha\beta}}{r_{ij}^6} + \frac{q_\alpha q_\beta}{4\pi\epsilon_0 r_{ij}} \quad (2)$$

$$U^{BOND}(r_{ij}) = \sum_{n=2}^{4} k_{\alpha\beta}^{BOND}(n)(r_{ij} - r_{\alpha\beta}^0)^n \quad (3)$$

$$U^{BEND}(\theta_{ijk}) = \sum_{n=2}^{4} k_{\alpha\beta\gamma}^{BEND}(n)(\theta_{ijk} - \theta_{\alpha\beta\gamma}^0)^n \quad (4)$$

$$U^{TORS}(\phi_{ijkl}) = -{}^1/_2 \sum_n k_{\alpha\beta\gamma\delta}^{TORS}(n)[1 + \cos(n\phi_{ijkl})] \quad (5)$$

where $r_{\alpha\beta}^0$ is the equilibrium bond length between atoms of type α and β; $\theta_{\alpha\beta\gamma}^0$ is the equilibrium bend angle between atoms of type, α, β, and γ; $k_{\alpha\beta}^{BOND}(n)$, $k_{\alpha\beta\gamma}^{BEND}(n)$, $k_{\alpha\beta\gamma\delta}^{TORS}(n)$, $A_{\alpha\beta}$, $B_{\alpha\beta}$, $C_{\alpha\beta}$, q_α, and q_β are the bond and bend force constants, torsion parameters, nonbonded parameters, and partial charges, respectively.

TABLE 3: Partial Atomic Charges (e) for PDMS and Model Compounds

atom	DS	HMDS	DMTS	OMTS	TMTS	PDMS
Si			0.7608	0.8612	0.8202	0.7608
Si[a]		0.8376		0.7780		0.6792
Si[b]	0.6316		0.7395		0.8131	
O	−0.4477	−0.5144	−0.4620	−0.5302	−0.5018	−0.4620
C		−0.5284	−0.5604	−0.4277	−0.5460	−0.5604
H		0.1117	0.1370	0.0861	0.1289	0.1370
H[b]	−0.1359		−0.1695		−0.1873	

[a] End silicon atom bonded to three methyl groups. [b] End silicon atom bonded to three hydrogen atoms.

The methodology followed in parametrization of the PDMS potential is described in greater detail below. Briefly, partial atomic charges were first determined for each oligomer of interest by fitting the electrostatic potential on a grid of points around model PDMS compounds obtained from quantum chemistry calculations. Next, nonbonded Buckingham potential (exp-6) parameters for silicon were determined by fitting the binding energies between a pair of SiH_4 molecules determined from high-level quantum chemistry calculations. Valence parameters (r^0, θ^0) were fit to obtain the best description of quantum chemistry geometries of the lowest-energy model compounds. Finally, dihedral parameters were determined by fitting conformational energetics of DMTS.

B. Electrostatic Partial Charges. Electrostatic partial charges were calculated by minimizing the $\Sigma(\varphi_i^{QC} - \varphi_i^{FF})^2$ objective function for the TMTS, DMTS, OMTS, HMDS, and DS molecules, where φ_i^{QC} and φ_i^{FF} are the electrostatic potentials at a grid point i from quantum chemistry calculations and from the force field, respectively.[13] The sum is taken over all grid points that extend from the van der Waals (VDW) radius of each atom to 4.0 Å from any atom. VDW radii of 2.0, 2.0, 2.5, and 1.8 Å were used for Si, O, C, and H, respectively. The electrostatic distribution of DS was calculated at the MP2/aug-cc-pvDz level of theory to most accurately represent the molecular dipole and HF/6-31G(2d) calculations were performed for the other model molecules. The partial atomic charges showed some dependence upon molecular weight and structure of the molecule. For example, the silicon partial charge was 0.63 e for DS but increased to ∼0.8 e for TMTS, OMTS, and HMDS due to the presence of the stronger electron-withdrawing (relative to hydrogen) methyl groups. The resulting partial charges for the model molecules are shown in Table 3. After comparing the charges of the most important oligomers, the charges from DMTS were used for the polymer molecule because the silicon and oxygen charges were closest to the average of all oligomers. The carbon and hydrogen charges are larger than those used in literature force fields.[14]

C. Silicon Nonbonded Parametrization. Our experience shows that the nonbonded (dispersion and repulsion) parameters for a particular atom type are reasonably transferable from one polymer to another, provided that the chemical environments are similar. Consequently, the validated nonbonded parameters for oxygen, carbon, and hydrogen parameters were taken from our previous force fields.[15] In past force fields, the carbon−hydrogen nonbonded interaction was parametrized separately, but in this force field, it was calculated using the standard combining rules (see below) consistent with the approach taken for all other nonbonded cross-terms. To establish repulsion and dispersion parameters for silicon, high-level quantum chemistry calculations were performed on a pair of silane (SiH_4) molecules. On the basis of previous experience, using the quantum chemistry HF and MP2 energies calculated for molecular pairs

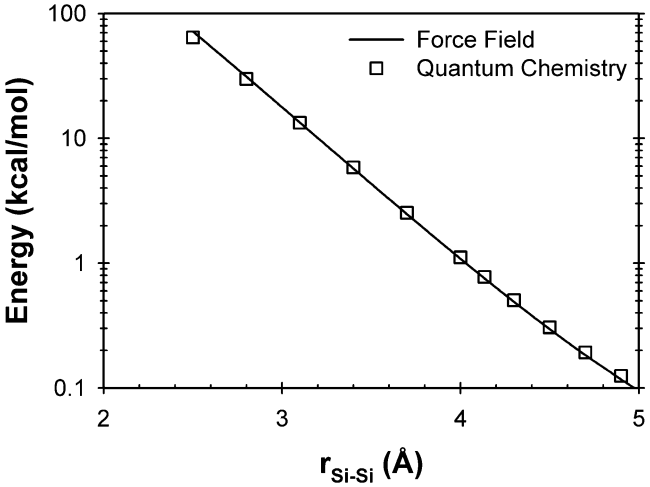

Figure 2. Hartree−Fock energy (HF/aug-cc-pvDz) between two silane molecules and the repulsive and electrostatic interaction energies (eq 2, $C_{\alpha\beta} = 0$) from the force field developed in this work.

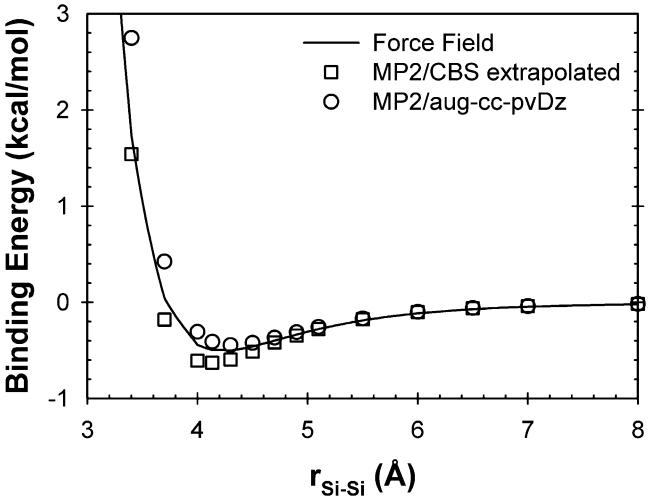

Figure 3. MP2/aug-cc-pvDz and MP2/CBS extrapolated binding energies for two silane molecules as a function of silicon atom separation. Also shown is the total binding energy (repulsive, dispersive, and electrostatic, eq 2) from the force field developed in this work.

with B3LYP optimized geometries and augmented correlation consistent double, triple, and quadruple-ζ basis sets, we have reproduced the intermolecular binding interaction between model molecules well. Therefore, the molecular geometry was determined for a single silane molecule at the B3LYP/aug-cc-pvDz level and was kept fixed for the calculations of the pair energies. The minimum energy configuration for the molecular pair was determined at the MP2/aug-cc-pvQz//B3LYP/aug-cc-pvDz level and was found to correspond to a silicon atom separation (r_{Si-Si}) of 4.135 Å.

The dimer binding energy was determined along the minimum energy path of closest approach between two silane molecules, varying only r_{Si-Si}, and is given as the difference between the basis set superposition error (BSSE) corrected (using the counterpoise method)[16] energy of the dimer and the energy of the isolated molecules. Typically, the most important contributions to the total binding energy between two molecules include intermolecular electrostatic, polarization, repulsion, and dispersion interactions. At small separations (less than the equilibrium separation), the intermolecular forces are repulsive and are generally ascribed to the electrostatic and repulsive interactions. The electrostatic potential on a grid of points surrounding a silane molecule was calculated at the MP2/aug-cc-pvDz level and was well represented with partial charges of 0.61 and −0.15 e for silicon and hydrogen, respectively. Hartree−Fock energies (HF/aug-cc-pvDz//B3LYP/aug-cc-pvDz) from quantum chemistry calculations include contributions from electrostatic and repulsive energies, and the linear dependence of the silane molecules HF level energy on silicon atom separation (semilog plot of Figure 2) indicates that an exponential function is most appropriate for description of repulsion in this region.[17] We therefore represented the HF/aug-cc-pvDz energy as a sum of intermolecular electrostatic and repulsive interactions (eq 2, $C_{\alpha\beta} = 0$), allowing us to determine the Si−Si repulsion parameters A_{SiSi} and B_{SiSi}. Repulsion parameters for Si−C, Si−H, and Si−O interactions were taken as $A_{SiX} = (A_{SiSi}A_{XX})^{1/2}$ and $B_{SiX} = 0.5*(B_{SiSi} + B_{XX})$, where X = C, H, or O, as given in Table 4. The combined SiH_4 dimer repulsive and electrostatic energy of this force field is also shown in Figure 2.

At larger separations, the intermolecular binding energy is primarily due to polarization, electrostatic, and dispersive interactions. Although the best method for calculating molecular dispersion remains unresolved in the literature,[18−20] in this work the dispersion interaction (correlation energy) between the SiH_4 molecules as a function of separation was determined using aug-cc-pvXz basis sets, with $X = 2$ (*D*), 3 (*T*), and 4 (*Q*), as the difference between the BSSE corrected dimer energies determined at the MP2 and HF levels. For each separation investigated, a linear extrapolation of the correlation energy as a function of X^{-3} was made to the complete basis set (CBS) limit.[21] The total binding energy, shown in Figure 3, was then given by the sum of the extrapolated correlation energy and the HF/aug-cc-pvQz energy. Note that the HF energy was found to be insensitive to the basis set size beyond double-ζ. The many-body polarization contribution to the silane molecular pair binding energy was estimated[22] and found to be negligible, being less than 0.02 kcal/mol at separations larger than 4 Å. Therefore, the total binding energy was represented as a sum of electrostatic and repulsion interactions (already parametrized) and dispersion interactions (eq 2), allowing us to determine C_{SiSi}, with $C_{SiX} = (C_{SiSi}C_{XX})^{1/2}$. The total binding energy including repulsive, dispersive, and electrostatic interactions from this force field are shown in Figure 3. The binding energy minimum from this work lies between that predicted by the MP2/aug-cc-pvDz (also shown in Figure 3) and MP2/CBS extrapolated energies. This is similar to other polymer force fields we have developed where nonbonded interaction energies between the aug-cc-pvDz and CBS limits were found to accurately describe the heats of vaporization and cohesive energy densities of the polymer melts.[18] All nonbonded parameters are included in Table 4.

D. Bond and Bend Parametrization. Geometries, linearization energies, and conformational energies for DMTS (Figure 1c), determined at the HF/6-31G(2d) level of theory, were used to parametrize the Si−O−Si bend linearization energy barrier, equilibrium bond lengths, and bend angles as well as the conformational energy surface. The bond and bend force field constants, $k_{\alpha\beta}^{BOND}$ and $k_{\alpha\beta\gamma}^{BEND}$, originally developed for the CFF force field,[14] were used except as noted in this section. The equilibrium bond lengths and bond angles, $r_{\alpha\beta}^0$ and $\theta_{\alpha\beta\gamma}^0$, listed in Table 4, were determined by multivariate optimization to best represent the geometries of the lowest-energy conformations of DMTS. The O−Si−O bend force constant was fit using a single quadratic term to represent the quantum chemistry energy of the *tt* conformer (with constrained torsions) of DMTS determined for various fixed values of the O−Si−O bend angle near the optimal angle. The C−H bond and H−C−H bend constants from our previous force fields were used, although

TABLE 4: Parameters for the Nonbonded and Bonded PDMS Potential

$$U^{NB}(r) = \sum_{i<j} A_{\alpha\beta} \exp(-B_{\alpha\beta} r_{ij}) - \frac{C_{\alpha\beta}}{r_{ij}^6} + \frac{q_\alpha q_\beta}{4\pi\epsilon_0 r_{ij}}$$

nonbonded interactions	A (kcal/mol)	B (Å^{-1})	C (kcal Å^6/mol)	source ref
Si−Si	50326	2.846	3085.3	this work
Si−O	61781	3.454	1109.4	combining rules[a]
Si−C	24753	2.968	1406.1	combining rules[a]
O−O	75844	4.063	398.9	ref 16
O−C	33702	3.577	505.6	combining rules[a]
O−H	14177	3.902	104.5	combining rules[a]
C−C	14967	3.090	640.8	ref 16
C−H	6300	3.415	132.5	combining rules[a]
H−H	2650	3.740	27.4	ref 16

$$U^{BOND}(r_{ij}) = \sum_{n=2}^{4} k_{\alpha\beta}^{BOND}(n)(r_{ij} - r_{\alpha\beta}^0)^n$$

bonds	$k^{BOND}(2)$ (kcal/mol/Å^2)	$k^{BOND}(3)$ (kcal/mol/Å^3)	$k^{BOND}(4)$ (kcal/mol/Å^4)	$r_{\alpha\beta}^0$ (Å)	$r_{\alpha\beta}^0$ (Å) (constrained)
Si−O[b]	350	−517	674	1.651	1.65
Si−C[b]	190	−279	308	1.878	1.88
C−H[c]	328			1.092	1.09

$$U^{BEND}(\theta_{ijk}) = \sum_{n=2}^{4} k_{\alpha\beta\gamma}^{BEND}(n)(\theta_{ijk} - \theta_{\alpha\beta\gamma}^0)^n$$

bends	$k^{BEND}(2)$ (kcal/mol/rad^2)	$k^{BEND}(3)$ (kcal/mol/rad^3)	$k^{BEND}(4)$ (kcal/mol/rad^4)	$\theta_{\alpha\beta\gamma}^0$ (deg)
Si−O−Si[d]	10.305	−18.101	10.100	137.63
O−Si−O	91.835			105.56
O−Si −C[b]	23.022	−31.399	24.981	109.82
C−Si−C[b]	36.210	−20.390	20.020	112.44
Si−C−H[b]	28.770	−13.950		111.09
H−C−H[c]	38.500			107.77

$$U^{TORS}(\phi_{ijkl}) = -{}^1/_2 \sum_n k_{\alpha\beta\gamma\delta}^{TORS}(n)[1 + \cos(n\phi_{ijkl})]$$

torsions	$k^{TORS}(1)$ (kcal/mol)	$k^{TORS}(2)$ (kcal/mol)	$k^{TORS}(3)$ (kcal/mol)
Si−O−Si−O[d]	−0.41000	0.27319	0.21968
Si−O−Si−C			−0.05706
O−Si−C−H			−0.15000
C−Si−C−H			−0.15000

[a] $A_{\alpha\beta} = (A_{\alpha\alpha}A_{\beta\beta})^{1/2}$; $B_{\alpha\beta} = (B_{\alpha\alpha} + B_{\beta\beta})/2$; $C_{\alpha\beta} = (C_{\alpha\alpha}C_{\beta\beta})^{1/2}$. [b] Bonded constants k^{BOND}, k^{BEND} are from ref 14. [c] Bonded constants k^{BOND}, and k^{BEND} are from ref 15. [d] Linearizing Si−O−Si Bend and Si−O−Si−O torsion are coupled by the following equation:

$$U^{TORS} = \frac{\sin^2(\theta_{ijk})}{\sin^2(\theta_{ijk}^0)} \times \sum_{n=1}^{3} -{}^1/_2 k_{\alpha\beta\gamma\delta}^{TORS}(n)(1 + \cos(n\phi_{ijkl}))$$

all bond lengths were constrained in molecular dynamics simulations (section VI.A).

The Si−O−Si bend is anharmonic and cannot be described by the usual quadratic potential function. Including cubic and quartic (anharmonic) terms allows for an accurate description of the linearization barrier from quantum chemistry calculations. It was found that the intramolecular 1,4 nonbonded interactions varied strongly with the Si−O−Si bend angle, making accurate representation of the linearization energy problematic. However, scaling the 1,4 intramolecular nonbonded interactions by 50% allowed us to obtain an adequate fit of conformational energetics and linearization of DMTS. The quadratic, cubic, and quartic force constants for the Si−O−Si bend were fit to give a reasonable representation of the energy of the *tt* constrained conformer of DMTS as a function of the Si−O−Si angle as both bends were linearized. A comparison of molecular mechanics and quantum chemistry from this bend fit is shown in Figure 4. The molecular mechanics of the Si−O−Si bend linearization energies for DMTS (*tt* geometry) and DMTS (*tcis* geometry) of 0.38 and 1.14 kcal/mol, respectively, are in good agreement with the quantum chemistry values of 0.37 and 1.47 kcal/mol determined at the HF/6-31G(2d) level. Linearization energy for the Si−O−Si bend of the larger OMTS (minimum geometry) and TMTS (*tcistcis* geometry) oligomers were 0.9 and 1.1 kcal/mol, respectively, compared with values of 1.6 and 1.8 kcal/mol from quantum chemistry at the HF/6-31G(2d) level.

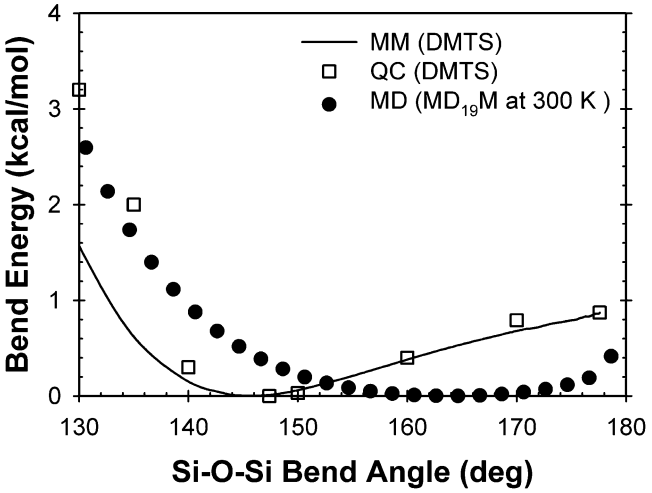

Figure 4. Comparison of molecular mechanics (MM) and HF/6-31G(2d) QC energies for simultaneously linearizing both Si−O−Si bends in a DMTS molecule (tt geometry), and the relative Si−O−Si bend angle free energy calculated from the MD simulation bend angle populations of $MD_{19}M$ chains at 300 K.

Therefore, there is reasonable transferrability of these parameters to larger compounds if the uncertainty of the HF/6-31G(2d) level of theory is considered.

E. Bend−Torsion Cross Terms. Linearization of the Si−O−Si bend can result in artifacts during molecular dynamics simulations of PDMS. When a Si−O−Si bend linearizes, the dihedral angles of the two backbone torsions containing that bend become undefined, resulting in a discontinuity in the dihedral energy and associated forces. To avoid this situation, we modified the dihedral potential for Si−O−Si−O torsions as follows:

$$U^{\mathrm{TORS}} = \frac{\sin^2(\theta_{ijk})}{\sin^2(\theta^0_{ijk})} \times \sum_{n=1}^{3} -{}^1/_2 k^{\mathrm{TORS}}_{ijkl}(n)(1+\cos(n\phi_{ijkl})) \quad (6)$$

where θ_{ijk} and θ^0_{ijk} are the angle and equilibrium angle of the Si−O−Si bend contained in the Si−O−Si−O type torsion. The sine-squared term scales the dihedral energy (and force) smoothly to zero as the Si−O−Si bend linearizes. To accurately reproduce the linearization energy and conformational energies in DMTS, an iterative procedure that involves first fitting the linearization energy by adjusting the Si−O−Si bend potential, followed by adjusting the Si−O−Si−O dihedral potential (see below) to fit the conformational energy surface, and then revisiting the linearization energy was required. Satisfactory convergence was obtained after three iterations.

F. Torsion Parametrization. Rotations of the SiH_3- and CH_3- groups exhibit threefold rotational symmetry. They were fit to end-group and methyl-group rotations of the DMTS molecule, and matched the HF/6-31G(2d) rotational barriers of 0.35 and 0.72 kcal/mol to within 0.02 and 0.04 kcal/mol, respectively. The C−Si−O−Si torsional parameters were obtained by matching the conformational energy associated with the trimethylsilyl group ($(CH_3)_3Si-$) rotation in an HMDS molecule (Figure 1b) determined at the HF/6-31G(2d) level. The relatively flat threefold symmetric conformational energy surface for this rotation is well represented by the force field, with respective minima and barrier at angle 120° with an energy of 0.11 kcal/mol.

The Si−O−Si−O torsional parameters were fit to provide the best representation of the conformational energies and geometries of DMTS for stationary points given in Table 2**,** as well as additional conformations not given in the table. In all, 28 conformations were used in the fitting. The HF/6-31G(2d) and MP2/6-311G(2df)//B3LYP/6-311G(2df) energies were used as upper and lower limits, respectively. The force field energies and geometries for the stationary points are given in Table 2. For most conformations, the force field energies lie within these upper and lower quantum chemistry bounds. The root mean square (rms) deviation of the force field energies from the HF/6-31G(2d) energies for all 28 conformers is 0.30 kcal/mol, while the deviation from the MP2/6-311G(2df) energies is 0.27 kcal/mol. When the mean of the HF/6-31G(2d) and MP2/6-311G(2df) energies for each conformation is compared with the force field energy for that conformation, the rms deviation reduces to 0.22 kcal/mol. As shown in Table 2, the geometry of the minimum-energy *cis*150 conformer is reproduced well by the force field. Finally, Figure 5 is a conformational energy map obtained for DMTS from molecular mechanics using the force field given in Table 4. The extreme flatness of the conformational energy surface for DMTS is apparent.

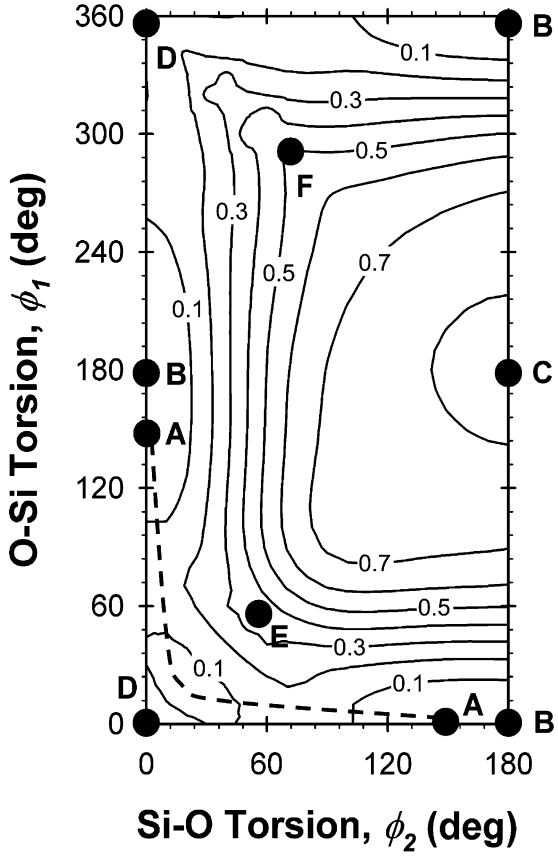

Figure 5. Contour plot comparing the dihedral energy surface of DMTS calculated from the force field developed in this work, with quantum chemistry data points marked with labels corresponding to the labels found in Table 2 for the HF/6-31G(2d) and MP2/6-311G(2df)//B3LYP/6-311G(2df) levels of theory (angles in degrees, contours in kcal/mol). The dashed line illustrates the low-energy path from one dyad minimum to the other.

IV. Validation of the Force Field

For purposes of validation of the quantum chemistry based potential for PDMS given in Table 4, molecular dynamics (MD) simulations were performed on melts of PDMS oligomers. Direct comparison of thermophysical, structural, and dynamic properties obtained from the simulations with experiment was undertaken.

A. Simulation Methodology. MD Simulations of ensembles of melts of 10 PDMS molecules ($MD_{19}M$, 19 repeat units each) with molecular weight (MW in g/mol), MW = 1571, 16 molecules ($MD_{10}M$, 10 repeat units) with MW = 904, 24 molecules (MD_6M, 6 repeat units) with MW = 607, and 43 molecules (MD_2M, 2 repeat units) with MW = 311, were performed at temperatures from 300 to 549 K. Throughout this paper and its figures, a shorthand notation is used where trimethylsiloxy ($(CH_3)_3SiO-$) monofunctional units are represented by the letter M, and the dimethylsiloxy ($-(CH_3)_2SiO-$) difunctional units by the letter D, with the number of repeat units in subscript.[23] All simulations were carried out with the *Lucretius*[24] MD simulation package using a Nose−Hoover thermostat[25] and barostat[26] to control the temperature and pressure with bond lengths constrained using the shake algorithm.[27] The particle mesh Ewald (PME) technique[28] was used to treat all electrostatic interactions. A multiple time-step reversible reference system propagator algorithm[26] was employed for all NVT and NPT production runs with a time step of 0.5 fs for bond, bend, and torsional motions, a 1.0 fs time step for all VDW and real electrostatic interactions within a sphere of radius 7.0 Å, and a 2.0 fs time step for nonbonded interactions in the shell between radii of 7.0 and 10.0 Å and for the reciprocal space PME calculations. Initially, the melts were created in the gas phase and run at 700 K for over 100 ps, then each melt was reduced to its final temperature. Next, they were equilibrated for 1000 ps in an NPT ensemble at 1 atm to give equilibrium box sizes. Additional 1000 ps high-pressure NPT runs at 395 and 1184 atm were made to determine the scaling of density with pressure. NVT production runs of 90 ns were undertaken at 300 K for all melts, and the average pressure was about -33 ± 20 atms.

Brownian dynamics simulations were performed on HMDS, MD_2M, and MD_6M in the gas phase (no intermolecular interactions) for 1 ns after 100 ps equilibration. Potential energy from these simulations was used in heat of vaporization calculations.

B. Conformational Characterization. The characteristic ratio, Si−O−Si bend angle distribution, the Si−O−Si−O dihedral angle distribution, and Si−O−Si−O−Si and O−Si−O−Si−O torsional dyad populations were calculated for the $MD_{19}M$ systems at 300 K. The characteristic ratio, C_∞, was estimated to be 5.5 by extrapolating calculations of C_N plotted vs N^{-1} to the ordinate axis, where N is the number of backbone bonds of length 1.651 Å. This is in excellent agreement with SANS data,[29] which estimates values of 5.7−5.8 for deuterated chains in a PDMS melt at 298 K and the wide spread of values, 5.7−7.6, measured in θ solvents.[30]

The relative free energy of the Si−O−Si bend angle, $V(\theta)$, was calculated from the bend angle populations, $p(\theta)$, according to the following:

$$p(\theta) = \frac{N_\theta}{\sin(\theta)\sum N_\theta} \tag{7a}$$

$$V(\theta) = -kT\ln(p(\theta)) \tag{7b}$$

where N_θ is the number of Si−O−Si bends with the angle θ and the probability function is normalized by $\sin(\theta)$. The results for $MD_{19}M$ chains simulated at 300 K are plotted in Figure 4, where the energy of the most probable bend angle (161°) was assumed to be zero. The relative energy of the bend linearization barrier appears to be 0.8 kcal/mol, but there is some uncertainty since the probability of finding angles scales as $\sin(\theta)^{-1}$ and could vary as much or more than ±0.3 kcal/mol very near linearization. The shift of the most probable Si−O−Si angle in the MD melt simulations ($MD_{19}M$ molecules) to a larger angle (relative to the DMTS molecule) reflects a more open structure for the longer chains possibly due to the bulkier CH_3 groups on the backbone.

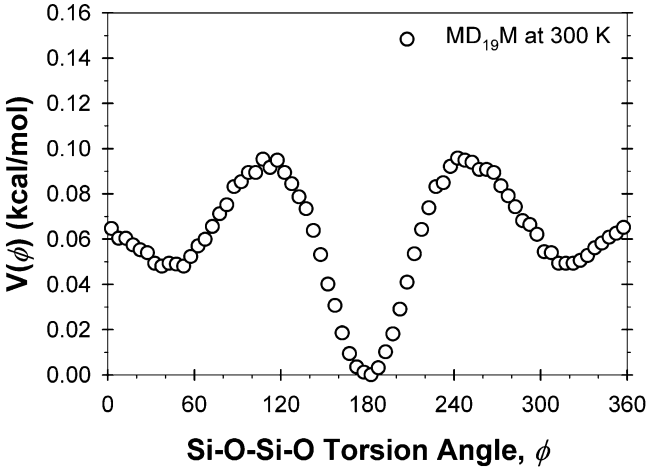

Figure 6. Backbone Si−O−Si−O-type relative torsional free energy barriers from MD simulation dihedral populations of $MD_{19}M$ chains at 300 K (angles in degrees).

The relative free energy of the backbone Si−O−Si−O dihedral as a function of dihedral angle was determined from the dihedral angle distribution:

$$V(\phi) = -kT\frac{p(\phi)}{p(180°)} \tag{8}$$

where $p(\phi)$ is the probability of finding the Si−O−Si−O torsion with angle ϕ. The relative free energy is shown in Figure 6. The extreme flatness of the conformational energy surface is clearly manifested in this nearly angle-independent free energy with a free energy barrier of only 0.1 kcal/mol.

Corresponding backbone dyad conformational energy surfaces, $V(\phi_1,\phi_2)$, were calculated from the torsional dyad populations, $p(\phi_1,\phi_2)$, of the MD simulations (see eq 7) for the silicon- and oxygen-centered dyads (illustrated in Figure 1, c and e, respectively) and are plotted in Figure 7. Some important features of the silicon-centered dyad surface (Figure 7a) include the flatness of the energy surface, minimum near *cist*, and symmetry with the low-energy path between minima (dashed line in Figure 7a) that all agree qualitatively with the molecular mechanics energy surface (Figure 5) for DMTS. The main differences between Figures 5 and 7a are the significantly lower *cis*−*cis* population (free energy barrier of 1.2 kcal/mol) that may be due to the longer-range steric effects that prohibit *cis*−*cis*−*cis* conformations and the slight increase in the *tt* population (shallow free energy minimum) that may be due to increased intermolecular interactions in the melt that favor more expanded local conformations. The oxygen-centered dyad energy surface (Figure 7b) shows minima near *cist*, a low-energy path between the minima and a relatively high *cis*−*cis* energy similar to the silicon-centered dyads (Figure 7a). Note that the quantum chemistry of the oxygen-centered dyads was not systematically studied because of the prohibitive size of the smallest representative compound. The high relative energy of the *tt* conformer precludes the formation of all *t* helixes consistent with the findings of others[31] and lowers the probability of *tt* sequences contrary to early PDMS RIS models of Flory, Crescenzi, and Mark.[32]

C. Thermodynamic Properties. The densities and specific volumes of PDMS oligomers from MD simulations with the

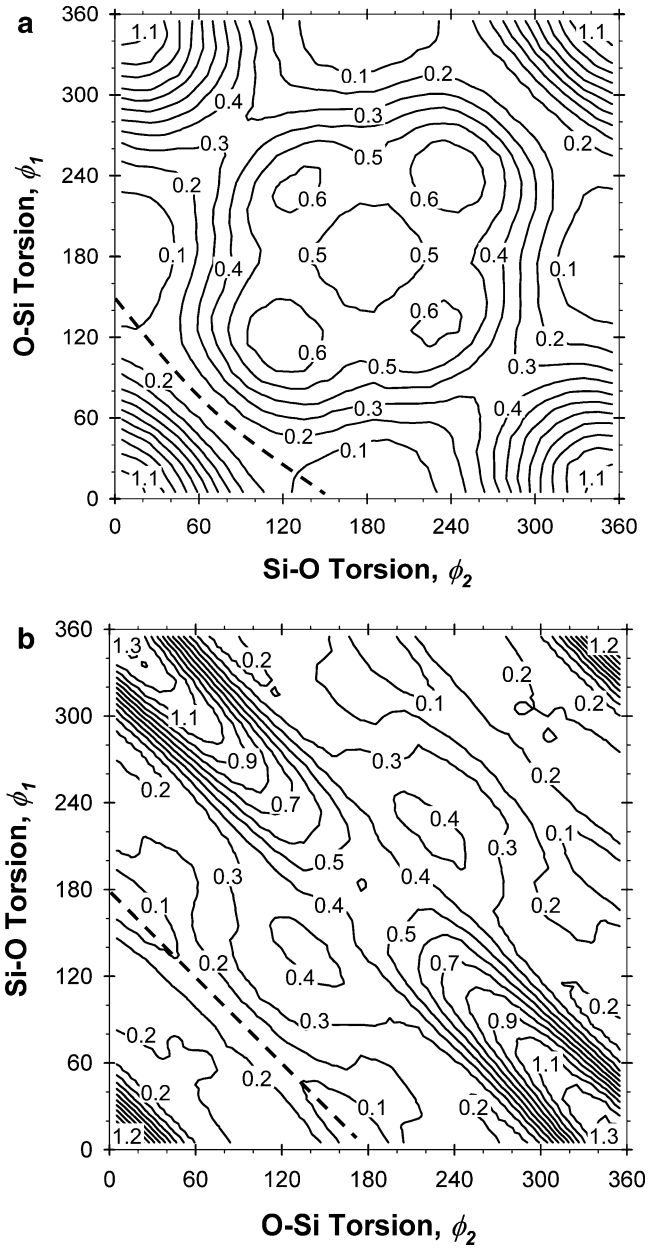

Figure 7. Torsional dyad relative free energy surfaces for (a) silicon-centered dyads and (b) oxygen-centered dyads calculated from MD simulation dyad populations of $MD_{19}M$ chains at 300 K (angles in degrees, contours in kcal/mol). Dashed lines illustrate the low-energy path from one dyad minimum to the other.

developed force field are shown in Figures 8, 9, and 10. Figure 8 shows the densities of several molecular weights for the force field developed in this work as well as some experimental values and data from literature force fields.[14] The new force field reproduces the experimental densities of Beevers et al.[33] for molecules from MD_2M to $MD_{19}M$ within 1.3% at 300 K and 1 atm pressure. The difference in experimental densities (which was greatest for low molecular weights) can be in part due to the difference in polydispersity ratios (M_w/M_n) of the samples that varied from 1.02 for the lowest molecular weight to 1.55 for the highest molecular weights tested at Los Alamos National Laboratory,[34] and only 1.00 to 1.02 for the experiments of Beevers et al.[33] Additional data reported in the book by Zoller and Walsh[35] (shown in Figure 8) agreed well with the data of Beevers et al.[33] for the short PDMS oligomers (viscosity average molecular weight of ~340, M_w/M_n = 1.02) but disagreed by over 3% for the longer oligomers (viscosity average molecular

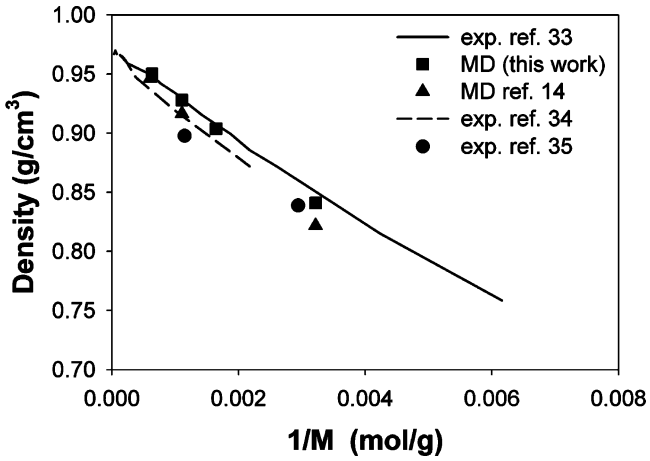

Figure 8. Comparisons of densities for the force field developed in this work and the CFF force field[14] with experimental values of Beevers et al.,[33] Los Alamos National Laboratory,[34] and Zoller and Walsh[35] over a range of molecular weights at atmospheric pressure and 300 K.

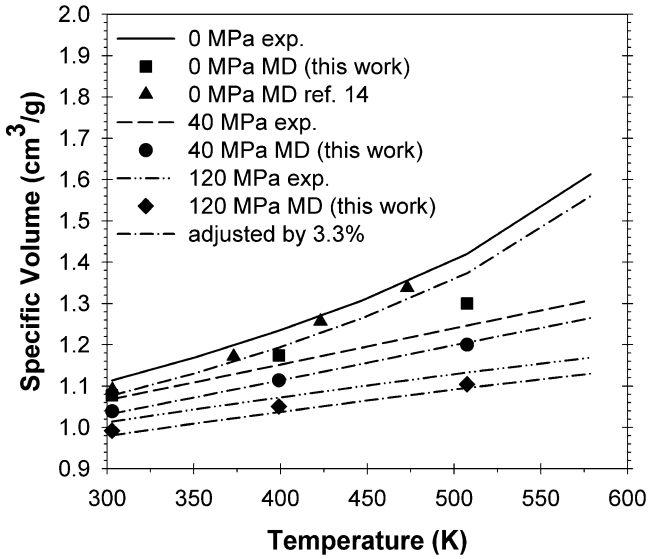

Figure 9. Comparison of specific volumes of $MD_{10}M$ (MW = 904) calculated using the force field developed in this work at pressures of 0, 40, and 120 MPa, and the CFF force field[14] at 0 MPa, with experimental measurements[35] of samples with MW ~870 from 300 to 579 K. The adjusted data represent the experimental specific volume data minus 3.3% (see section IV.C).

weight of ~870, M_w/M_n of 1.13) because of the higher polydispersity of the samples.

Comparison of the specific volume calculated using the force field and experimental values (Zoller and Walsh[35]) are shown in Figures 9 and 10 for a range of temperatures and pressures. The density of the smallest oligomers, MD_2M, was within 3% of experimental results for chains at temperatures up to 400 K and ambient pressure. Calculations at 542 K and 1 atm pressure, which is between the reported normal boiling point at 479 K and critical point of 599 K (at 10 atm),[36] were meaningless due to finite size effects inherent to the simulations and showed a 22% deviation. Densities improved and were within 1.8% for experiments at 395 and 1184 atm (40 and 120 MPa) pressure for temperatures ranging from 300 to 542 K. The same was not true for simulations of $MD_{10}M$ oligomers where the density was overestimated by 3−5% over similar temperature and pressure ranges when compared with Zoller and Walsh's experimental data (MW ~870, M_w/M_n= 1.13).[35] When the data of Zoller and Walsh[35] was recalibrated to account for its polydispersity by simply shifting the specific volume curves

TABLE 5: Heat of Vaporization, Self-Diffusion Coefficient, and Viscosity of PDMS and its Oligomers

	heats of vaporization (kcal/mol)		self-diffusion coefficient (10^{-6} cm^2/s)		viscosity (centipoises)	
compound	simulation[a]	experiment[b]	simulation[a]	experiment[c]	simulation[a]	experiment[d]
HMDS	9.1	9.1 (0%)[e]				
MD_2M	14.9	15.1 (1%)	3.2 ± 0.3	1.96−7.0	2.2 ± 0.5	1.31−1.51
MD_6M	28.6	26.8 (−6%)	0.68 ± 0.06	0.93	7.0 ± 0.9	3.69−3.94
$MD_{10}M$			0.33 ± 0.02	0.63	9.0 ± 2.5	5.57−6.6
$MD_{19}M$			0.10 ± 0.01	0.37	21.0 ± 5.0	11−13

[a] All simulations were performed at 300 K. [b] Experimental data in ref 36 at 300 K. [c] Experimental self-diffusion coefficients from refs 40 and 41 at 293 and 298 K respectively. [d] Experimental viscosities from refs 40 and 42 at 298 K. [e] Deviation of simulation values from experiment.

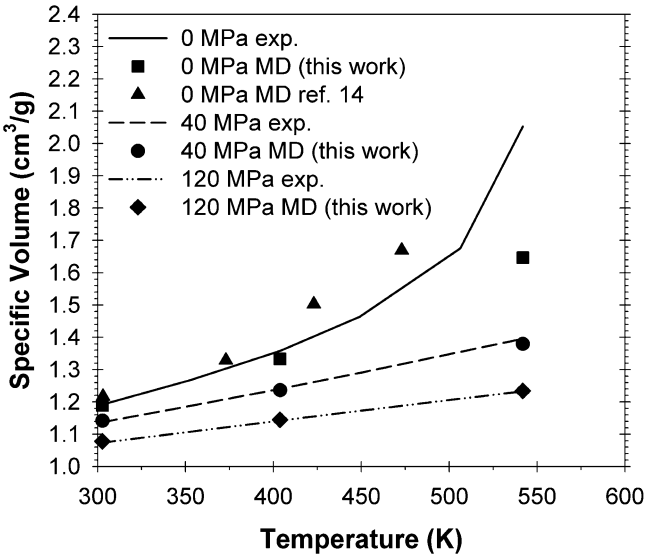

Figure 10. Comparison of specific volumes of MD_2M (MW = 311) calculated using the force field developed in this work at pressures of 0, 40, and 120 MPa, and the CFF force field[14] at 0 MPa, with experimental measurements[35] of samples with MW ~340 from 300 to 542 K.

by about 3.3% to match the 300 K data reported by Beevers et al.,[33] as shown in Figure 9, the $MD_{10}M$ molecules with the new force field reproduce the densities to within 2% for temperatures up to 400 K at 1 atm pressure, and within 1% at the higher pressures for temperatures from 300 to 508 K.

Heats of vaporization were calculated for hexamethyldisiloxane, decamethyltetrasiloxane, and octadecamethyloctasiloxane using melt-state and gas-state simulations at standard temperature and pressure. The molecular dynamics and experimental results are compared in Table 5. The HMDS, MD_2M, and MD_6M results are in good agreement with values calculated from experimental vapor pressures[36] using the Clausius−Clapeyron equation.

D. Comparison of X-ray Structure Factor. The X-ray structure factor $H(k)$ was also calculated using radial distribution functions according to the formula:[37]

$$H(k) = 1 + \frac{n}{\langle |b_\alpha(k)|^2 \rangle} \sum_{\alpha\beta} x_\alpha b_\alpha(k) x_\beta b_\beta(k) \times \int_0^{r_c} [g_{\alpha\beta}(r) - 1] \frac{\sin kr}{kr} 4\pi r^2 \mathrm{d}r \quad (9a)$$

$$\langle |b_\alpha(k)|^2 \rangle \equiv \sum_\alpha x_\alpha |b_\alpha(k)|^2 \quad (9b)$$

where $b_\alpha(k)$ denotes the k-dependent atomic form factor $f_\alpha(k)$ for species α; $g_{\alpha\beta}(r)$ is the pair distribution function between species α and β, with concentrations, x_α and x_β, respectively, and the cutoff radius, r_c, is 15 Å; n is the number density. The structure factors for $MD_{19}M$ at 300 K and X-ray measurements reported in the literature[38] are shown in Figure 11. Good agreement is found between the MD simulation and experimental X-ray structure factors, indicating that the developed force field captures PDMS structure correctly.

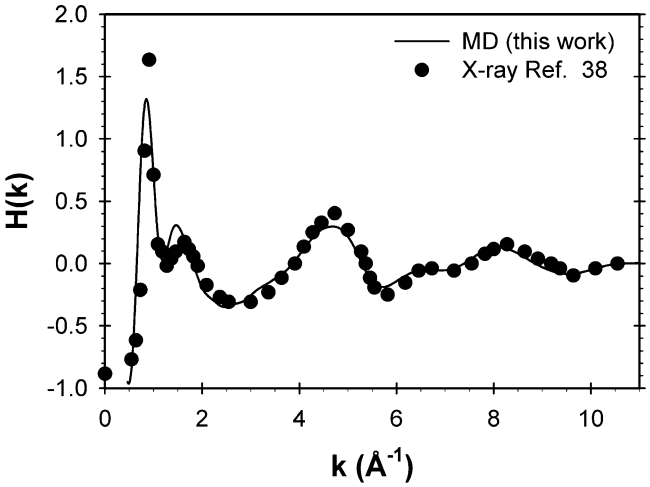

Figure 11. Comparison of the X-ray structure factors calculated from MD simulations of $MD_{19}M$ chains with experimental data at 300 K.[38]

E. PDMS Dynamics: Self-Diffusion and Viscosity. The dynamics of PDMS was validated by investigating the self-diffusion, viscosity, and motion of PDMS hydrogen atoms measured through the incoherent intermediate structure factor decay. The self-diffusion coefficient D is calculated using the Einstein relation:[39]

$$D = \lim_{t\to\infty} \frac{\langle R^2(t) \rangle}{6t} \quad (10)$$

where $\langle R^2(t) \rangle$ is the mean square displacement of a molecule center of mass during time t, and $\langle\ \rangle$ denotes an ensemble average. The self-diffusion coefficients from simulation and experiments[40] at 293 K are compared in Table 5. The agreement between experiment and simulation for the self-diffusion coefficient is reasonable, becoming somewhat poorer with increasing molecular weight. Note, however, that, on the basis of multiple measurements[40,41] for the lowest molecular weight compounds, uncertainties in the reported values for all molecular weights may be relatively large.

The viscosity is calculated using the Einstein relation[39]

$$\eta = \lim_{t\to\infty} \frac{V}{6k_B T t} \langle \langle \sum_{\alpha\neq\beta} (L_{\alpha\beta}(t) - L_{\alpha\beta}(0))^2 \rangle \rangle \quad (11a)$$

$$L_{\alpha\beta}(t) = \int_0^t P_{\alpha\beta}(t')\mathrm{d}t' \quad (11b)$$

where k_B is the Boltzmann constant, T is temperature, t is time, $P_{\alpha\beta}$ is the symmetrized stress sensor, and V is the volume of

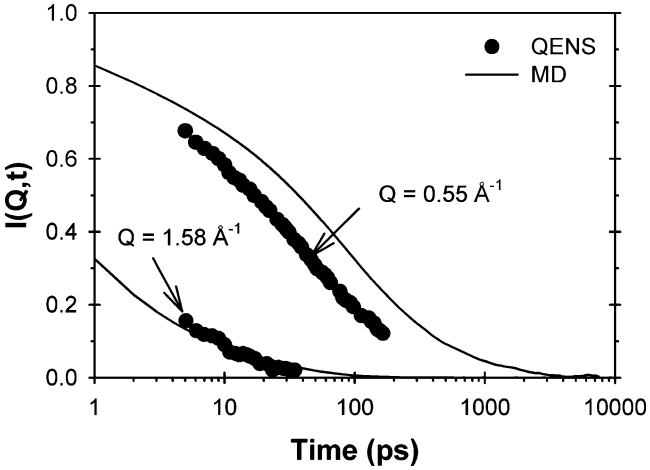

Figure 12. Comparison of $I(Q,t)$ calculated from MD simulations of $MD_{19}M$ (MW 1571) at 300 K and measured from QENS experiments[43] (MW 93 000) at 303 K.

the simulation box. The calculated viscosities and range of experimental values[42] at 298 K are shown in Table 5. The viscosities were uniformly higher than the experimental values and showed poorer agreement as the molecular weight increased similar to the self-diffusion coefficient data.

F. PDMS Dynamics: Intermediate Incoherent Dynamic Structure Factor. The local dynamics of the PDMS chains were probed by quasi-elastic neutron scattering (QENS) experiments at 303 K.[43] The intermediate incoherent structure factor (IISF) data of a high molecular weight (MW = 93 000) PDMS melt from QENS experiments are available for two Q values (0.55 and 1.58 Å) and are shown in Figure 12. The IISF was calculated from simulation trajectories using eq 12:[44]

$$I(Q,t) = \left\langle \frac{\sin(\Delta r_i(t)Q)}{\Delta r_i(t)Q} \right\rangle \qquad (12)$$

where $\Delta r_i(t)$ is the displacement of atom i after time t, Q is the magnitude of the momentum transfer vector, and $\langle\ \rangle$ denotes an average over all time origins for atoms with a significant incoherent cross section (i.e., hydrogen atoms).

The match between the experiment and simulation IISF is excellent for $Q = 1.58$ Å^{-1}, demonstrating the ability of the force field to reproduce the local molecular motions attributed primarily to methyl rotations in the chain. At $Q = 0.55$ Å^{-1}, the simulations predict roughly 2 times slower dynamics than QENS experiments. The slower dynamics seen at $Q = 0.55$ Å^{-1} is consistent with the lower self-diffusion coefficient and higher viscosities of $MD_{10}M$ and $MD_{19}M$ predicted by simulations.

V. Discussion

Early MD simulations[45] used general force fields such as CHARMM, and in 1996, Huai Sun and David Rigby of Molecular Simulations[14] developed a polysiloxane force field (herein referred to as CFF) based on ab initio calculations using the functional forms of the consistent force field that was included in the subsequent COMPASS[46] force field. Recently, a new united atom force field[47] has been made by combining and empirically adjusting the parameters of the CFF force field and an earlier united atom force field[48] to obtain the best agreement with the explicit atom CFF force field for the structure factor, density, and chain dimensions of PDMS. No heat of vaporization or any dynamic properties have been calculated for this new united atom force field. Therefore, it cannot be considered more accurate than the CFF force field, and our discussion will focus on the CFF force field. The CFF force field was parametrized mainly on ab initio calculations at the HF/DZ2P level of theory on DS, silanol, dimethylsilane, dimethylsilanol, disilanol, and trisiloxane model compounds. MD liquid simulations of DS, 1,3-disilyl-disiloxane, HMDS, and MD_2M molecules were used to make empirical adjustments to the CFF nonbonded parameters. Much more consideration was given during validation to reproducing vibrational frequencies.

The force field developed in this work was parametrized also using HMDS and several larger and more complex model compounds at a higher level of quantum chemistry (see section II). The dispersion parameter for the Si−Si interaction derived from quantum chemistry done on the silane molecule (section III.C) is 20% higher, but the H−H dispersion interaction used in parametrization was 30% lower than those found in the CFF, and overall, our partial charges were slightly higher.

The density and specific volume calculations with our current force field were generally in better agreement with experiment in Figures 8, 9, and 10 than those of CFF. The notable exceptions occur for the smallest MD_2M compounds at temperatures above ~500 K at 1 atm pressure, which as noted before is above the boiling point and near the critical point of the liquid, and for $MD_{10}M$ above 400 K at 1 atm pressure. To match those densities, the CFF authors had to reduce the electrostatic cutoff of their simulations from 11.5 to 8.5 Å, artificially destabilizing the liquid at the higher temperatures; in fact, at the 11.5 Å cutoff, the densities showed underestimation of the specific volume at high temperatures. The heats of vaporization (or closely related cohesive energy density and solubility parameters) from the present force field were in excellent agreement with experiment and much better than CFF for the MD_6M molecule. The agreement in structure factors for the force field developed in this work was similar to calculations done by Sides et al.[38] for MD simulations of $MD_{18}M$ molecules done using the CFF force field when the ensemble density was constrained to 0.98 g/cm^3 at 298 K. There is no published CFF data for comparison of the self-diffusion coefficient, viscosities, and incoherent intermediate structure factors.

VI. Conclusions

Systematic investigations showed that the important disiloxane Si−O−Si bend characteristics of PDMS oligomers at the HF/6-31G(2d) level fit well into the range of experimental bend angle and linearization energy barrier values. Because of this, and its computational efficiency, the HF/6-31G(2d) and MP2/6-311G(2df) levels were used to investigate several oligomers, most extensively the DMTS molecule, and revealed a relatively flat conformational energy surface for the backbone dihedrals. The classical force field resulting from this work reproduced well, both in single-molecule molecular mechanics and MD multiple chain melt simulations, these important backbone bend and dihedral energies and conformations with a bend−dihedral coupling that suppressed any problems with MD energy and force calculations that can arise from the lability of the Si−O−Si bend.

The resulting structure factors from MD simulations of PDMS melts with the new force field were in good agreement with experimental data at 300 K. The densities of PDMS scaled well with molecular weight at 300 K and continued to match experiments within 3% up to 400 K at ambient pressure and compared as favorably over even a wider range of temperatures

at higher pressures. The heats of vaporization and chain dimensions (C_∞) were in agreement with experimental thermodynamics and SANS measurements. All of these results were as good as or quantitatively better than data reported from MD melt simulations done using previous PDMS force fields.[14]

The dynamic behavior of the PDMS and oligomer melts were in good agreement with experimental self-diffusion coefficients, viscosities, and intermediate incoherent structure factor data. Despite poorer agreement with experimental dynamics as molecular weight increased, overall it was satisfying to see such agreement from a force field where the silicon nonbonded, Si−O−Si and O−Si−O bend, and dihedral parameters were based wholly on quantum chemistry data with no empirical adjustments to nonbonded parameters as was done in previous force fields in the literature.

Acknowledgment. We would like to acknowledge funding through the Department of Energy, Los Alamos National Laboratory, Contract 79277001032F, and use of their computational resources.

References and Notes

(1) Mark, J. E. Silicon-Containing Polymers. In *Silicon-Based Polymer Science*; Zeigler, J. M., Fearon, F. W. G., Eds.; Advances in Chemistry Series 224; American Chemical Society: Washington DC, 1990; p 47.

(2) Sun, C.-C.; Mark, J. E. *Polymer* **1989**, *30*, 104.

(3) Berrod, G.; Vidal, A.; Papirer, E.; Donnet, J. B. *J. Appl. Polym. Sci*. **1981**, *26*, 833.

(4) Almenningen, A.; Bastiansen, O.; Ewing, V.; Hedberg, K.; Traetteberg, M. *Acta Chem. Scand.* **1963**, *17*, 2455. Lord, R. C.; Robinson, D. W.; Schumb, W. C. *J. Am. Chem. Soc.* **1957**, *78*, 1327.

(5) Aronson, J. R.; Lord, R. C.; Robinson, D. W. *J. Chem. Phys.* **1960**, *33*, 1004.

(6) Csonka, G. I.; Reffy, J. *Chem. Phys. Lett.* **1994**, *229*, 191.

(7) Grigoras, S.; Lane, T. H. *J. Comput. Chem.* **1987**, *8*, 84.

(8) Nicholas, J. B.; Winans, R. E., Harrison, R. J.; Iton, L. E.; Curtiss, L. A.; Hopfinger, A. J. *J. Phys. Chem.* **1992**, *96*, 7958.

(9) Koput, J. *J. Phys. Chem.* **1995**, *99*, 15874.

(10) Frisch, M. J.; Trucks, G. W.; Schlegel, H. B.; Scuseria, G. E.; Robb, M. A.; Cheeseman, J. R.; Zakrzewski, V. G.; Montgomery, J. A., Jr.; Stratmann, R. E.; Burant, J. C.; Dapprich, S.; Millam, J. M.; Daniels, A. D.; Kudin, K. N.; Strain, M. C.; Farkas, O.; Tomasi, J.; Barone, V.; Cossi, M.; Cammi, R.; Mennucci, B.; Pomelli, C.; Adamo, C.; Clifford, S.; Ochterski, J.; Petersson, G. A.; Ayala, P. Y.; Cui, Q.; Morokuma, K.; Malick, D. K.; Rabuck, A. D.; Raghavachari, K.; Foresman, J. B.; Cioslowski, J.; Ortiz, J. V.; Stefanov, B. B.; Liu, G.; Liashenko, A.; Piskorz, P.; Komaromi, I.; Gomperts, R.; Martin, R. L.; Fox, D. J.; Keith, T.; Al-Laham, M. A.; Peng, C. Y.; Nanayakkara, A.; Gonzalez, C.; Challacombe, M.; Gill, P. M. W.; Johnson, B. G.; Chen, W.; Wong, M. W.; Andres, J. L.; Head-Gordon, M.; Replogle, E. S.; Pople, J. A. *Gaussian 98*, rev A.7; Gaussian, Inc.: Pittsburgh, PA, 1998.

(11) Koput, J.; Wierzbicki, A. *J. Mol. Spectrosc.* **1983**, *99*, 116.

(12) *cis* = 0°, *t* = trans = 180°, g^+ = gauche = 60°, g^- = gauche = 300°.

(13) Borodin, O.; Smith, G. D. *J. Chem. Phys.* **2003**, *107*, 6801. Breneman, C. M.; Wiberg, K. B. *J. Comput. Chem.* **1990**, *11*, 361.

(14) Sun H.; Rigby D. *Spectrochim. Acta, Part A* **1997**, *53*, 1301.

(15) Sorensen, R. A.; Liau, W. B.; Kesner, L.; Boyd R. H. *Macromolecules*, **1988**, *21*, 200. Smith, G. D.; Jaffe, R. L.; Yoon, D. Y. *J. Phys. Chem.* **1993**, *97*, 12752.

(16) Boys, S. F.; Bernardi, F. *Mol. Phys.* **1970**, *19*, 553.

(17) Using molecular mechanics, we calculated the total electrostatic contribution to the binding energy and found that it was less than 10% at distances less than 3.8 Å, indicating that repulsion (A, B) parameters account for most of the energy at the HF/aug-cc-pvDz level at these distances.

(18) Calculations of noble gas dimer dispersion (ref 19) using augmented Dunning basis sets at the MP2, MP4, and CCSD(T) levels of theory showed increasingly close agreement with experimental well depths, and the agreement at all levels of theory was better when complete basis set estimations were used. Recent work on small molecules representative of the functional groups of organic materials (ref 20) suggested that the use of a large number of diffuse functions (augmented sets) leads to an overpolarization of the molecular liquids and violation of Pauli exclusion in the condensed phase, both of which lead to an overestimation of the dielectric constants and heats of vaporization. Our own investigations of PEO and small alkane molecules at the MP2 level have shown that augmented double-ζ calculations underestimate dispersion but that the complete basis set expansion can in many instances overestimate it.

(19) Woon, D. E. *J. Chem. Phys.* **1994**, *100*, 2838.

(20) Kaminski, G. A.; Stern, H. A.; Berne, B. J.; Freisner, R. A. *J. Phys. Chem. A* **2004**, *108*, 621.

(21) Smith, G. D.; Borodin, O.; Bedrov, D. *J. Comput. Chem.* **2002**, *23*, 1480. Halkier, A.; Klopper, W.; Helgaker, T.; Jorgensen, P.; Taylor, P. R. *J. Chem. Phys.* **1999**, *111*, 9157.

(22) We estimated the many-body polarization contribution to the SiH_4−SiH_4 binding energies using molecular mechanics calculations of the dimer with quantum chemistry based partial charges and isotropic atomic polarizabilities. Atoms within the same molecule were excluded from direct interactions. Partial charges were obtained by fitting the MP2/aug-cc-pvDz electrostatic potential around SiH_4, whereas the isotropic atomic polarizabilities were fit to the polarization energy due to a test charge (1e). Polarization energy was calculated as the difference between the energy of $SiH_4/q = 1e$ complex minus the electrostatic potential calculated at the MP2/aug-cc-pvDz level.

(23) Hurd, C. B. *J. Am. Chem. Soc.* **1946**, *68*, 364.

(24) Smith, G. D.; Ayyagari, C.; Bedrov, D.; Borodin, O. *Lucretius*; http://lucretius.mse.utah.edu/, 2004.

(25) Nose, S. In *Computer Simulations in Materials Science*; Meyer, M., Pontikis, V., Eds.; Kluwer Academic Publishers: Dordrecht, The Netherlands, 1991; p 21.

(26) Martyna, G. J.; Tuckerman, M. E.; Tobias, D. J.; Klein, M. L. *Mol. Phys.* **1996**, *87*, 1117.

(27) Ryckaert, J. P.; Ciccotti, G.; Berendsen, H. J. C. *J. Comput. Phys.* **1977**, *23*, 327.

(28) Deserno, M.; Holm, C. *J. Chem. Phys.* **1998**, *109*, 7678.

(29) Fetters, L. J.; Lohse, D. J.; Richter, D.; Witten, T. A.; Zirkel A.; *Macromolecules* **1994**, *27*, 4639. Beltzung, M.; Picot, C.; Rempp, P.; Herz, J. *Macromolecules* **1982**, *15*, 1594.

(30) Crescenzi, V.; Flory, P. J. *J. Am. Chem. Soc.* **1964**, *86*, 141. Zilliox, J. G.; Roovers, J. E. L.; Bywater S. *Macromolecules* **1975**, *8*, 573. *Polymer Handbook*, 4th ed.; Brandrup, J., Immergut, E. H., Grulke, E. A., Eds.; John Wiley & Sons: New York, 1999; Vol. VII, p 64.

(31) Darsey, J. A. *Macromolecules* **1990**, *23*, 5274.

(32) Flory, P. J.; Crescenzi, V.; Mark, J. E. *J. Am. Chem. Soc.* **1964**, *86*, 146.

(33) Beevers, M. S.; Mumby, S. J.; Clarson, S. J.; Semlyen J. A. *Polymer* **1983**, *24*, 1565.

(34) Kober, E. Private communication.

(35) Zoller, P.; Walsh, D. J. *Standard Pressure-Volume Temperature Data for Polymers*; Technonic: Lancaster PA, 1995; p 271.

(36) Flaningam, O. L. *J. Chem. Eng. Data* **1986**, *31*, 266.

(37) Ahlstrom, P.; Borodin, O.; Wahnstrom, G.; Wensink, E. J. W.; Carlsson, P.; Smith, G. D. *J. Chem. Phys.* **2000**, *112*, 10669.

(38) Sides, S. W.; Curro, J.; Grest, G. S.; Stevens, M. J.; Soddemann, T.; Habenschuss, A.; Londono, J. D *Macromolecules* **2002**, *35*, 6455.

(39) Haile, J. M. *Molecular Dynamics Simulations*; Wiley: New York, 1992; p 297.

(40) Cosgrove T.; Griffiths, P. C.; Hollingshurst, J.; Richards, R. D. C.; Semlyen, J. A. *Macromolecules* **1992**, *25*, 6761.

(41) McCall, D. W.; Huggins C. M. *Appl. Phys. Lett.* **1965**, *7*, 153.

(42) Hunter, M. J.; Warrick, E. L.; Hyde, J. F.; Currie, C. C. *J. Am. Chem. Soc.* **1946**, *68*, 2284. Dodgson, K.; Bannister, D. J.; Semlyen, J. A. *Polymer* **1980**, *21*, 663. Semlyen, J. A. In *Siloxane Polymers*; Clarson, S. J., Semlyen, J. A., Eds.; PTR Prentice Hall: Englewood Cliffs, 1993; p 166.

(43) Arrighi, V.; Ganazzoli, F.; Zhang, C.; Gagliardi, S. *Phys. Rev. Lett.* **2003**, *90*, 058301.

(44) Higgins, J. S.; Benoît, H. C. *Polymers and Neutron Scattering*; Clerendon Press: Oxford, 1996.

(45) Bahar, I.; Zuniga, I.; Dodge, R.; Mattice, W.L. *Macromolecules* **1991**, *24*, 2986.

(46) Sun, H. *J. Phys. Chem. B* **1998**, *102*, 7338.

(47) Frischknecht, A. I.; Curro, J. G. *Macromolecules* **2003**, *36*, 2122.

(48) Sok, R. M.; Berendsen, H. J. C.; van Gunsteren, W. F. *J. Chem. Phys.* **1992**, *96*, 4699.